Pergamon

Geochimica et Cosmochimica Acta, Vol. 64, No. 23, pp. 3933–3948, 2000

0016-7037/00 $20.00 + .00

PII S0016-7037(00)00483-X

Carbonate-mineral/water interactions in sulfide-rich mine tailings

TOM A. AL,[1,*] CHRIS J. MARTIN,[2] and DAVID W. BLOWES[3]

[1]Department of Geology, University of New Brunswick, P.O. Box 4400, Fredericton, NB, Canada, E3B 5A3
[2]Sunshine Mining and Refining Co., P.O. Box 1080, Big Creek Road, Kellogg, ID, 83837 USA
[3]Department of Earth Sciences, University of Waterloo, Waterloo, ON, Canada, N2L 3G1

(*Received November* 5, 1999; *accepted in revised form June* 9, 2000)

Abstract—The chemical composition and mineralogy of coatings on carbonate minerals from mine tailings have been studied using aqueous geochemical methods, Time-of-Flight Laser-Ionization Mass Spectrometry (TOF-LIMS) and Transmission Electron Microscopy (TEM). The goal is to study major and trace element partitioning between the aqueous and solid phase, and to infer mechanisms that control the concentrations of elements in the pore water of sulfide-rich mine tailings. Pore-water samples and carbonate-mineral grains were collected from four geochemically distinct zones within the tailings. Oxidation of sulfide minerals near the surface results in a large range in pore-water pH (3.85 to 6.98) and aqueous concentrations of metals and sulfate. With increasing depth in the tailings, mineral-water interactions lead to increasing pH, and decreasing concentrations of metals and sulfate. Calculated mineral saturation indices, trends in the abundance of Ca, Fe, Mg and Mn in TOF-LIMS profiles through the secondary coatings, and electron diffraction patterns obtained from the coatings, suggest that precipitation/dissolution of jarosite-group minerals, gypsum, goethite, akaganéite, amorphous Fe oxyhydroxides and siderite control the aqueous Ca, Fe, Na, K and SO_4 concentrations. The occurrence of secondary coatings on primary minerals is widespread, and reactions with the secondary minerals, rather than the primary mineral substrate, probably represent the principal controls on trace-element distributions in the pore water. The data indicate that adsorption, surface-complexation and co-precipitation reactions are important controls on the concentrations of trace elements in the pore water. The occurrence of siderite coatings on the surface of ankerite grains suggests that Fe-bearing dolomite-structure carbonate minerals dissolve incongruently. This corroborates inferences made by previous workers that solubility differences between calcite and siderite lead to calcite dissolution and siderite precipitation during acid neutralization. The accumulation of secondary coatings will diminish the rate of mineral-dissolution reactions involving the primary minerals. Consequently, the use of kinetic rate constants obtained from the literature for simulating the dissolution of primary mineral phases such as the carbonates and alumino-silicates will likely overestimate the actual rates.

1. INTRODUCTION

Carbonate minerals such as calcite [$CaCO_3$], dolomite [$CaMg(CO_3)_2$], ankerite [$Ca(Fe,Mg)(CO_3)_2$] and siderite [$FeCO_3$] occur in association with a wide variety of economic mineral deposits, but from an environmental management perspective, the occurrence of carbonate minerals is particularly important in sulfide-bearing mineral deposits. The waste rock and tailings that remain following the extraction of metals from this type of ore commonly contain significant amounts of latent acidity in the form of Fe-sulfide minerals (e.g., pyrite [FeS_2] and pyrrhotite [$Fe_{1-x}S$]). In the waste materials at mine sites, this latent acidity is gradually transformed to H^+ through sulfide-mineral, and ferrous-iron oxidation by atmospheric O_2. If carbonate minerals are present in the waste, their dissolution helps to prevent the formation of low-pH drainage from the waste containment areas.

When the pH of infiltrating water declines as a result of $Fe^{(II)}$ and sulfide oxidation, the concentrations of metals in the pore water (e.g., Fe, Al, Cu, Pb, Zn, Cd) commonly increase as a result of mineral-dissolution reactions. With continued infiltration below the zone of active sulfide oxidation, acid neutralization by carbonate minerals in tailings causes a reduction in the concentrations of dissolved metals (Dubrovsky et al., 1985; Blowes et al., 1991; Al et al., 1994a) because in the neutral pH range, most of these metals partition from the aqueous phase to mineral surfaces due to precipitation, co-precipitation and adsorption processes (Xu et al., 1997). The surfaces of carbonate minerals are highly reactive (Stipp and Hochella,1991), and co-precipitation and adsorption reactions at carbonate-mineral surfaces are likely to influence the concentrations of dissolved metals in these systems (Morin and Cherry, 1986; Bruno et al., 1998). Many investigators have described trace-element interactions at the surfaces of carbonate minerals, these interactions involve the formation of discreet trace-element carbonate overgrowths (Zachara et al., 1989; Chiarello and Sturchio, 1994), the co-precipitation of trace elements with carbonate minerals (Mucci and Morse, 1983; Wang and Merino, 1992; Dietzel and Usdowski, 1996; Tesoriero and Pankow, 1996; Chiarello et al., 1997; Rimstidt et al., 1998), and the adsorption or surface complexation of trace elements at the carbonate-mineral surface (Davis et al., 1987; Charlet et al., 1990; Zachara et al., 1991; Xu et al., 1996; Cheng et al., 1997; Sturchio et al., 1997; Brady et al., 1999). These types of investigations are typically conducted in controlled experimental systems with single carbonate phases in contact with defined aqueous solutions. In natural systems such as mine tailings, the mechanisms of trace-metal interactions with the carbonate-mineral surface are likely to be more complex, and the details are largely unknown. The purpose of this work is to relate the geochemistry of tailings

*Author to whom correspondence should be addressed (tal@unb.ca).

pore water, and the chemical composition of the surfaces of carbonate minerals collected from various depths within a tailings dump, to the mineralogy of secondary coatings at the carbonate surfaces. This approach is intended to assist the development of conceptual and numerical models of reactive transport in tailings and waste-rock pore water.

2. REACTIONS AT CARBONATE-MINERAL SURFACES IN SYSTEMS INFLUENCED BY SULFIDE OXIDATION

The common conceptual model for reactions between carbonate minerals and pore water in sulfide-rich mine tailings and waste rock is one where carbonate minerals gradually dissolve under the influence of acidity derived from sulfide oxidation. Field and experimental evidence indicates that the order of dissolution of the Ca- Mg- Fe-carbonate minerals is calcite, followed by dolomite, ankerite and finally siderite (Blowes and Ptacek, 1994; Jurjovec et al., 1995). Blowes and Ptacek (1994) observed that during dissolution, the pore water is commonly near equilibrium with respect to calcite and siderite. Blowes and Ptacek (1994) also noted that pore waters are commonly undersaturated with respect to dolomite and ankerite, suggesting that dissolution of dolomite and ankerite is kinetically inhibited.

In addition to carbonate-mineral dissolution reactions, positive saturation indices have commonly been observed for siderite in mine-tailings pore water where Fe is released to the pore water by sulfide-mineral oxidation (Dubrovsky et al., 1985; Morin and Cherry, 1986; Al et al., 1994a; Blowes and Ptacek, 1994). This observation has lead authors to suggest that secondary siderite may precipitate in this environment; however, evidence of secondary siderite precipitation in mine wastes is rare. The occurrence of secondary siderite on the surface of ankerite collected from a mine tailings dump was confirmed by Al et al. (1997).

There are few reported investigations of the relationship between dissolved concentrations of trace elements and the carbonate mineralogy in mine tailings and waste rock systems. Carbonate minerals have an indirect influence on trace-element concentrations by neutralizing metal-rich low-pH pore water, leading to adsorption and co-precipitation of trace elements with insoluble $Fe^{(III)}$ and Al oxides, hydroxides and sulfates (Blowes et al., 1991; Robbins et al., 1999; Cravotta and Trahan, 1999). It is logical to assume that, at the microscopic level, a variety of secondary-mineral coatings are present at the surface of the carbonate minerals, with the specific nature of the coatings governed by the ambient pH, redox condition and pore-water composition. Such coatings may have a strong influence on the trace-element composition of the groundwater, and they limit the interaction of dissolved metals with the surface of the primary carbonate mineral to diffusion-controlled mass transfer. This hypothesis is supported by experiments conducted by Booth et al. (1997) in which polished calcite surfaces were exposed to 0.1 M H_2SO_4 solutions in a flow-through reactor and the dissolution rate of calcite was observed to decline to a low asymptotic value over a period of only 17 min. Following these experiments, analysis of the calcite surface using atomic force microscopy revealed a uniform coating of gypsum [$CaSO_4 \cdot 2H_2O$] crystals. On the basis of aqueous geochemical evidence, Morin and Cherry (1986) concluded that precipitation of siderite, or replacement of calcite by siderite, is responsible for retarding the transport of acidity and dissolved metals in a groundwater system that is recharged by mine-tailings pore water. Although geochemical investigations of tailings pore water commonly suggest that pore waters are in local equilibrium with the principal carbonate minerals (Blowes and Ptacek, 1994), at present there is little direct evidence to suggest that trace-element concentrations are controlled, or influenced directly by co-precipitation or solid-solution incorporation in carbonate minerals.

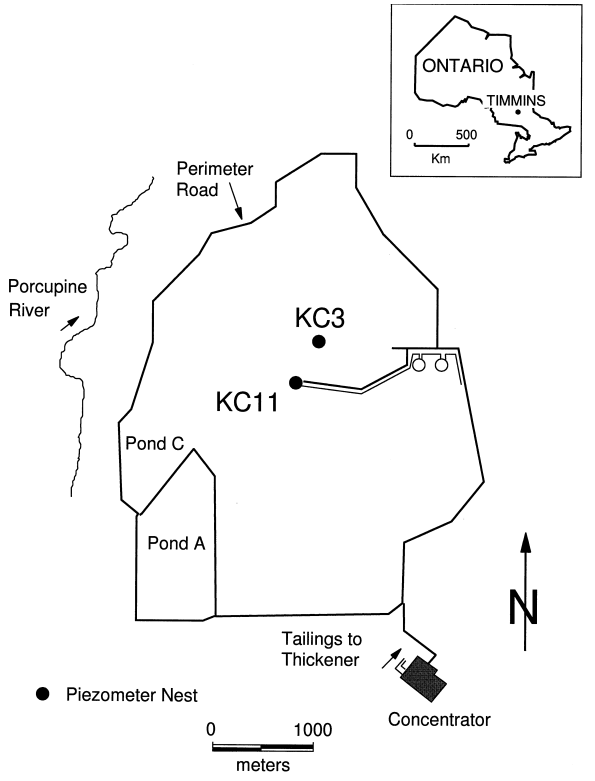

Fig. 1. Plan of the Kidd Creek tailings impoundment showing the locations of the piezometer nests where core samples were collected for this study.

Martin et al. (1997) compared the abundances of Pb and As at the surfaces of pyrite and carbonate minerals (siderite and ankerite/dolomite) collected from various depths within a tailings dump. The trends in Pb and As abundances at the mineral surfaces versus pH are consistent with a surface-complexation or adsorption mechanism for trace-element attenuation at the mineral surface. However, the surface analytical method that was used (Time-of-Flight Laser-Ionization Mass Spectrometry) can not identify secondary-mineral coatings at the carbonate-mineral surface. This paper extends the work of Martin et al. (1997), and it is demonstrated below that their results can not be interpreted simply in terms of interactions between the tailings pore water and the primary carbonate mineral surfaces.

3. SITE DESCRIPTION

The Kidd Creek tailings impoundment is 25 km east of Timmins, Ontario (Fig. 1). The tailings consist of 10 to 20 weight percent (wt%) pyrite, 1 to 2 wt% pyrrhotite, 1 to 2 wt%

combined sphalerite and chalcopyrite, and 75 to 85 wt% non-sulfide minerals. The most abundant of the non-sulfide minerals are quartz, biotite, hornblende and other silicates, and about 8 wt% carbonate minerals, dominated by siderite, ferroan dolomite and ankerite, with lesser amounts of calcite (Jambor et al., 1993).

Since 1985, a hydronium-bearing natrojarosite [$(Na,H_3O)Fe_3(SO_4)_2(OH)_6$] residue, derived from the zinc-refining process, has been blended with the tailings prior to disposal in the impoundment. In addition to Na, Fe, and SO_4, the natrojarosite residue contains variable amounts of As, Pb, Zn, K, Cd, Co, Cr, and other metals. Tailings in the upper 1 to 4.5 m of the impoundment contain an average of 2.5 wt% natrojarosite. The distribution of natrojarosite in the Kidd Creek impoundment and its effect on pore-water chemistry were described by Al et al. (1994a,b).

The distribution of metals and sulfate in the tailings pore water is dependent on the nature of the pore-water flow regime and the locations of solute sources. Pore-water flow within the Kidd Creek tailings has been described by Al et al. (1994b), and Al and Blowes (1996), Al and Blowes (1999). The central elevated portion of the tailings impoundment represents an area of net infiltration, wherein pore-water moves downward from the impoundment surface. Sample location KC11 (Fig. 1) is within this area. With increasing distance outward from the center of the impoundment, the pore-water flow changes from vertically downward to horizontal, directed toward the perimeter of the impoundment. Velocities are lowest in the deep pore water distant from the center of the impoundment, such as at sample location KC3. The locations of samples with respect to the positions of the water table and the zone of unsaturated tailings are shown in Figure 2.

Sources of solutes in the Kidd Creek tailings include sulfide oxidation, which is limited to the unsaturated zone near the impoundment surface, and dissolution of the natrojarosite present in the upper 1 to 4.5 m of tailings. These sources are stationary, and the solutes released to the pore water are transported downward by infiltrating pore water. Four pore-water geochemical zones (Fig. 3) can be defined within the Kidd Creek tailings (Al et al., 1994a,b). The pore water near the surface (up to 0.3 m deep) has been affected by sulfide oxidation, and the pore water at intermediate to shallow depths has been affected by the dissolution of natrojarosite. The dissolution zone may be subdivided into an upper zone containing natrojarosite, and a lower zone in which natrojarosite is absent, but in which solutes derived from natrojarosite dissolution are present. The pore water in the deep tailings is similar in composition to the mill discharge-water.

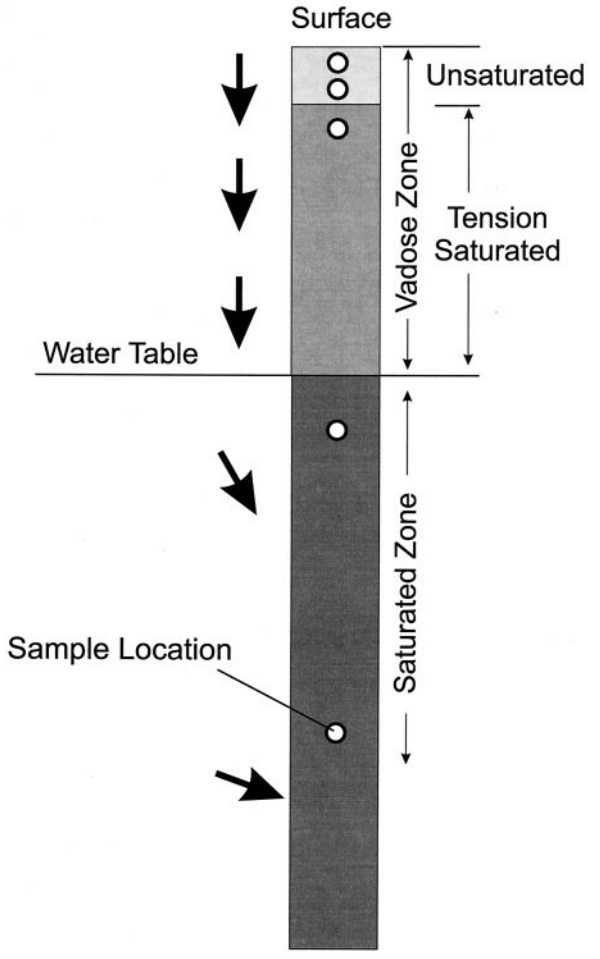

Fig. 2. Schematic representation of the hydrologic conditions at the tailings sample locations. The thickness of unsaturated tailings corresponds to the zone of sulfide-mineral oxidation (sample locations A and B). The arrows represent the groundwater flow direction.

4. METHODS

4.1. Sample Collection

4.1.1. Tailings pore water

Pore water was collected from the vadose zone and from the saturated zone of the tailings at piezometer nests KC11 and KC3, respectively (Fig. 1). Complete details of the pore-water sampling procedures, and analytical methods used, are provided by Al et al. (1994a). At the time of sampling, the tailings near the surface had been exposed to the atmosphere for approximately four years and the surficial tailings were visibly oxidized. In the vadose zone at KC11, where weathering reactions cause significant changes over time in pore-water pH and ion concentrations, the pore water was sampled at the same time that core samples were collected for the mineral-surface study. The aqueous geochemical data presented for the saturated zone at KC3 were collected one year prior to collection of the core samples, but it was demonstrated that the pore-water chemistry at KC3 was constant and reproducible for a two-year period prior to collecting the cores (Al, unpublished data).

To evaluate the tendency for secondary-mineral precipitation from the pore water, and the extent of aqueous complex formation, the geochemical equilibrium model MINTEQA2 (Allison et al. 1991) was used with a revised thermodynamic database from Ball and Nordstrom (1991).

4.1.2. Collection and treatment of carbonate minerals

Of the five samples (A to E in Fig. 3), three are from piezometer nest KC11 (A to C) and two are from piezometer nest KC3 (D and E). There is a well developed sulfide-oxidation zone at KC11. The pore-water flow is dominantly downward and is uncomplicated by horizontal gradients. The three samples from KC11 were collected from near the surface of the tailings in the sulfide-oxidation zone (A, 5 cm depth), from near the base of the zone (B, 15 cm depth), and from below the sulfide-oxidation zone but within the natrojarosite-containing zone (C, 55 cm depth). Of the two samples collected from piezometer nest KC3, one is from the zone where natrojarosite is absent but in which products

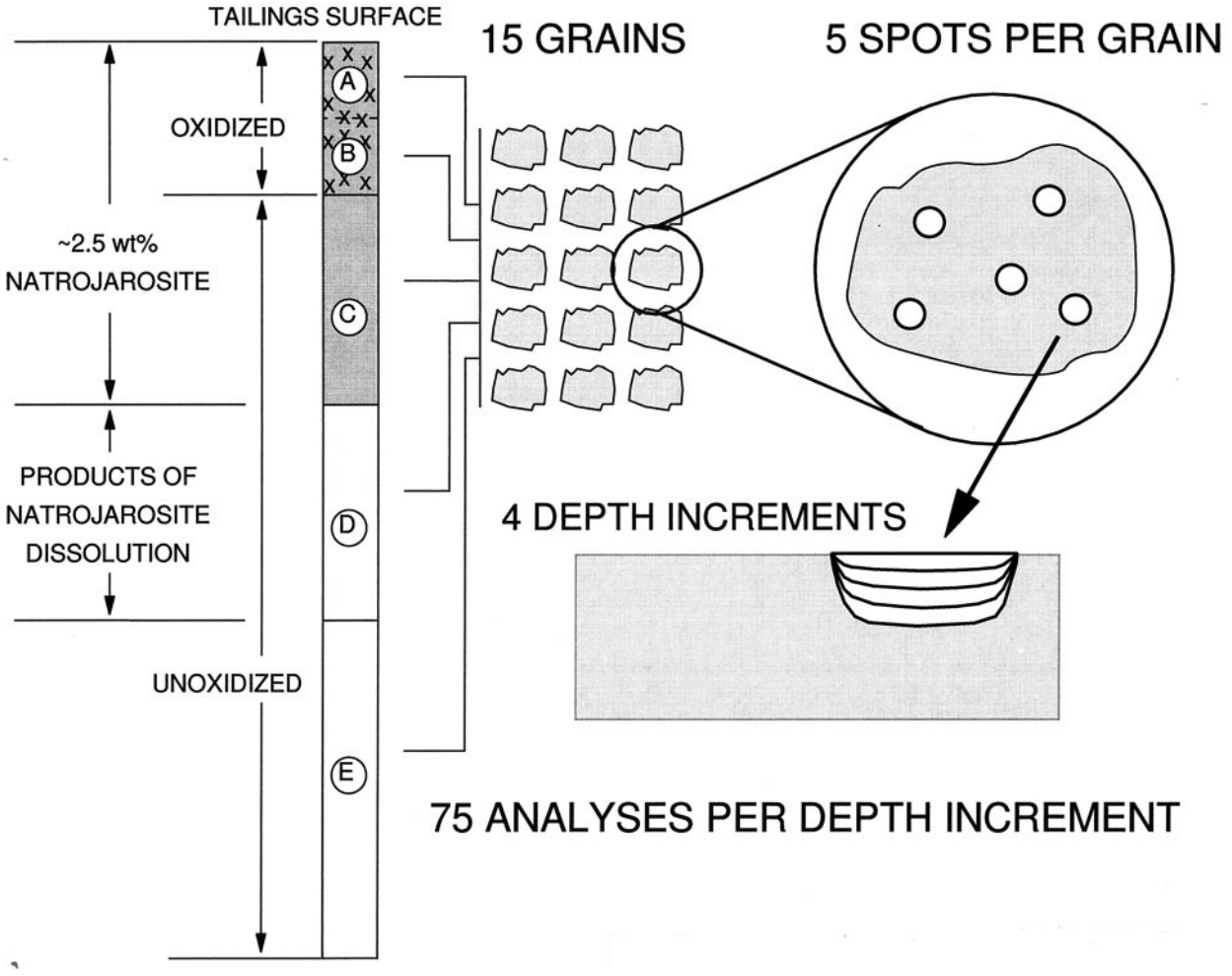

Fig. 3. Schematic diagram showing the sample locations for carbonate-mineral grains and pore water with respect to the stratigraphic level in the tailings. Also shown is the method used to analyze the surfaces of the grains. For each sampled zone within the tailings stratigraphy (A to E), the method results in 75 individual analyses for each depth increment.

of natrojarosite dissolution are present in the pore water (natrojarosite-affected zone, D, 400 cm depth), and the other sample is from the mill discharge-water zone (E, 800 cm depth).

Core samples were collected from the tailings impoundment in 5 cm diameter aluminum tubing. The core tube was cut into 10 cm intervals and each section was sealed on the top and bottom by a plastic cap and tape. The samples from piezometer nest KC3 (Fig. 1) were collected in June, 1992, and were frozen until August 1994. The cores from piezometer nest KC11 were collected in July, 1994 and were immediately taken to a field laboratory. In the lab, the tailings were extracted from the core tube and rinsed repeatedly with de-ionized water (at least 5 times) to remove the clay fraction and traces of the tailings pore water to prevent precipitation of secondary phases during drying. The samples were rinsed in methanol, oven-dried for 8 h. at 150°C and then sealed in double-wall plastic bags for temporary storage. The samples from KC3 were thawed and treated similarly.

Siderite, ferroan dolomite and ankerite are the principal carbonate minerals in the tailings. To recover individual grains of these minerals from the tailings samples, a Frantz Isodynamic Separator (Model L-1) was used to concentrate the sample by removing the silicate minerals with low magnetic susceptibility, and to separate siderite from ferroan dolomite and ankerite. X-ray diffraction was used to confirm the separation of siderite from ferroan dolomite and ankerite. Although ankerite and ferroan dolomite (hereinafter referred to collectively as ankerite) grains were targeted for this study, a few siderite grains were included. These grains were in the sample from the upper sulfide-oxidation zone where siderite is dominant. Using a steel needle, 15 carbonate-mineral grains, 50 to 100 μm in diameter, were picked from samples B to E. It was possible to recover only five grains from sample A. Samples were stored in a desiccator prior to further analysis.

4.2. Mineral Surface Analyses

4.2.1. TOF-LIMS

Surface analysis was conducted using a Time-of-Flight Laser-Ionization Mass Spectrometer manufactured by Cambridge Mass Spectrometry (model LIMA 2A). A detailed description of the instrument and its operation is provided by Odom and Schueler (1987); Odom and Schueler (1990).

The instrument is equipped with two Nd-YAG lasers (Quanta Ray, 266 nm wavelength; 4 ns pulse length). The first laser is directed perpendicular to the surface of the particle and ablates a sample from the top 20 to 100 Å of the particle surface. The ablation laser is focused to an analytical spot of 2 to 4 μm diameter, and is located on the particle surface using a coaxial He-Ne laser. Metallic species in the plasma cloud from the surface ablation are predominantly uncharged (ratio of charged particles to neutral particles is less than 10^{-4}; Odom and Schueler, 1987). The second laser has a diameter of approximately 250 μm and is directed parallel to the mineral surface 1.2 μs after the primary ablation laser. The second laser breaks molecular bonds in the plasma cloud and ionizes elements in the plasma. The ablation laser is

operated at 2.5×10^9 W/cm^2, and the post-ablation ionization laser is operated at 10^{10} W/cm^2.

An electrostatic field is maintained adjacent to the particle surface by applying a positive charge to the surface. Positively charged ions are repelled from the surface and are further accelerated and focused using electrostatic lenses prior to entering the TOF drift tube. The resulting time-resolved spectrum is calibrated using known peaks. The mass resolution of the TOF mass spectrometer is approximately 250, which is sufficient to resolve isotopes of all elements (Odom and Schueler, 1990). This resolution is not sufficient to distinguish ion clusters from single isotopes, for example $^{28}Si_2^+$ and $^{56}Fe^+$ or $^{32}S_2^+$ and $^{64}Zn^+$. Interferences from ion clusters are evaluated by monitoring elemental isotopic ratios. In many cases, such interferences may be avoided by selecting isotopes, such as $^{66}Zn^+$, that are not affected. The isotopic masses used to collect the data are presented with the results.

The carbonate grains were placed on indium-foil-plated aluminum mounts for TOF-LIMS analysis. Analyses were obtained for five spots on each of the fifteen carbonate grains (75 analyses) collected from each zone within the tailings section (Fig. 3). Removal of the surface material by laser ablation results in a crater typically 20 to 100 Å deep, exposing a subsurface layer which was analyzed by repeating the ablation procedure. The analytical results are presented in Figure 4 in terms of four depth increments. The second, third and fourth depth increments represent, respectively, three, six and ten ablation steps below the surface of the grain. An example of a mass-resolved spectrum for similar analyses of pyrite grains from the Kidd Creek tailings obtained by Al et al. (1997) is included in Figure 5. Al et al. (1997) conducted tests to determine possible changes in the surface composition that may have resulted from the water-rinse, methanol-rinse, and oven-drying steps during preparation of pyrite grains for surface analysis. Their results showed no systematic effects that could be related to sample preparation, except that the relative abundance of Pb on the surface is approximately 25 to 50% lower for the grains treated with methanol. Therefore, the reported relative abundance of Pb on the mineral surfaces may be underestimated, but the trends should not be affected because all samples were treated alike.

4.2.2. Transmission Electron Microscopy (TEM)

Individual carbonate-mineral grains were embedded in LR-White resin and sections 50 to 100 nm in thickness were prepared using a diamond-knife ultramicrotome. The sections were mounted on a formvar-coated nickel grid. All imaging, electron diffraction and energy dispersive X-ray analysis was conducted with a Philips EM400T TEM operated at an accelerating voltage of 120 KeV, and equipped with a LINK eXL X-ray analyzer. The TEM camera constant was calibrated daily using a thallous chloride diffraction standard (Agar Aids, S110).

The procedure for identifying secondary mineral coatings involved:

1. identifying discrete coatings on the surface of primary carbonate minerals using TEM imaging;
2. energy dispersive X-ray spectroscopic (EDS) analysis of the coating to determine the major-element components of the mineral coating;
3. obtaining a selected area electron diffraction pattern (SAED), or convergent beam electron diffraction pattern (CBED) from the coating, the method dependent on the thickness of the coating;
4. identifying the mineral and indexing the diffraction pattern by using the results of the EDS analysis, the NIST/SANDIA/ICDD electron-diffraction database and utilities, and the ICDD, PDF-2 database.

5. RESULTS

5.1. Pore-Water Geochemistry

In the mill discharge-water zone within the tailings (below 5 m at KC3 and below 9 m at KC11), the pore water has low concentrations of Fe, Mg, Mn, Na, K, HCO_3 and SO_4; most other metals are below detection (Table 1). The pH is near neutral and the E_H is between 100 and 200 mV. In the natrojarosite-containing, and natrojarosite-affected zones within the tailings (0.2 to 5 m at KC3 and 0.3 to 9 m at KC11), the pH is between 6.5 and 7 and the E_H is between 100 and 150 mV. Within these zones there are increased concentrations of Fe, Mg, Mn, Si, Na, K, Zn and Pb relative to the pore water in the deeper tailings (Table 1). In the sulfide-oxidation zone (above 0.3 m at KC11), the pore-water pH is lowest, the E_H is highest, and the pore water contains high concentrations of Mg, Mn, Si, Zn, Pb and SO_4 (Table 1) relative to the pore water in the deeper tailings. In addition, detectable concentrations of metals such as Al, Cu, Cd, Co, Ni and Cr are observed only in the sulfide-oxidation zone.

Geochemical speciation calculations suggest that free ions and sulfate complexes are the dominant forms of metals in the tailings water. Hydrolyzed species comprise a significant fraction of the total dissolved metals only for Al and Fe(III). Model calculations suggest that hydrolyzed species are present at low concentrations for the transition metals and alkaline earth metals.

The pore water in the sulfide-oxidation zone is saturated to supersaturated with respect to jarosite [$KFe_3(SO_4)_2(OH)_6$] and natrojarosite [$NaFe_3(SO_4)_2(OH)_6$] (upper sulfide-oxidation zone only), and is undersaturated with respect to hydronium jarosite [$(H_3O)Fe_3(SO_4)_2(OH)_6$] (Table 2). This water also is near saturation with respect to amorphous ferric hydroxide [$Fe(OH)_3$]. Oxidation of the tailings results in orange-yellow coloration in the sulfide-oxidation zone, indicating the formation of secondary ferric-iron minerals. Goethite [αFeO(OH)] was the only ferric-iron mineral identified by powder X-ray diffraction analyses of samples from the oxidized zone in the Kidd Creek tailings (Jambor et al., 1993). The pore water is supersaturated, by several orders of magnitude, with respect to the crystalline ferric oxyhydroxide minerals goethite and lepidocrocite [γFeO(OH)]. Calculations indicate that the pore water in this zone is undersaturated with respect to all other metal hydroxides. Alkalinity measurements were below detection, and the pore water is assumed to be undersaturated with respect to all carbonate minerals. In the lower sulfide-oxidation zone (B in Figs. 3 and 4), the pore water approaches saturation with respect to anglesite [$PbSO_4$]. The pore water throughout the tailings approaches or attains saturation with respect to gypsum [$CaSO_4 \cdot 2H_2O$]. Mineralogical studies indicate that gypsum is present throughout the tailings (Jambor et al., 1993).

Below the sulfide-oxidation zone (zones C to E) there are several changes in the calculated saturation indices. Saturation indices for $Fe(OH)_3$ and goethite are several orders of magnitude higher (Table 2). Despite the increase in pH, the pore water remains undersaturated with respect to the Cu and Ni hydroxides. Calculated saturation indices for carbonate minerals suggest that the pore water is undersaturated with respect to calcite, dolomite, magnesite, cerussite [$PbCO_3$], gaspéite [$NiCO_3$] and otavite [$CdCO_3$]. The pore water is near saturation with respect to siderite, rhodochrosite [$MnCO_3$] and smithsonite [$ZnCO_3$].

5.2. Mineral-Surfaces: TOF-LIMS Analyses

The relative abundances of elements at the mineral surface are presented in the form of count ratios of the ion signal from a particular element to the total ion signal:

$$\text{Count Ratio of } ^{208}\text{Pb} = \frac{\text{Number of } ^{208}\text{Pb Counts}}{\text{Total Number of Counts}}$$

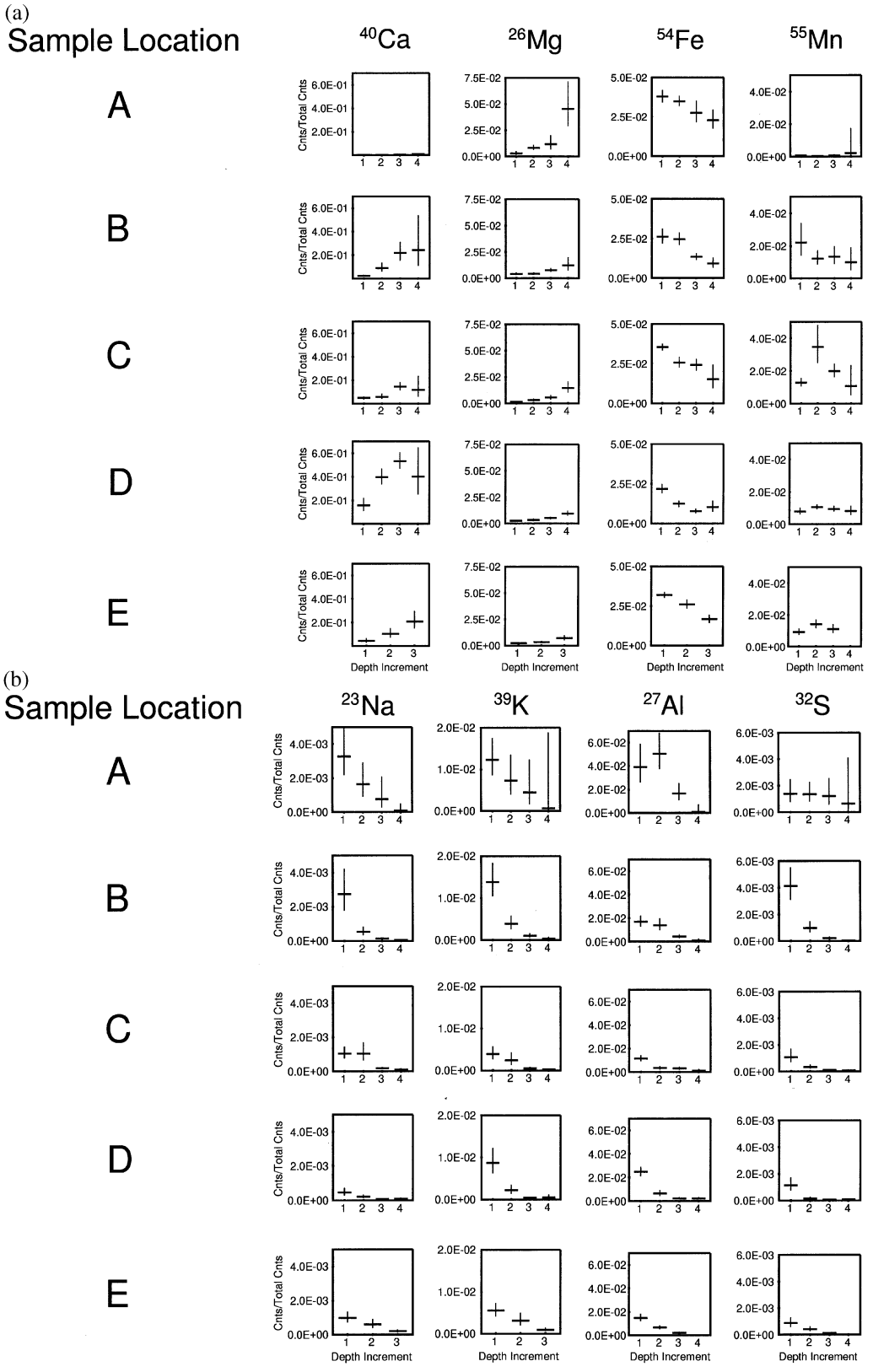

Fig. 4. Results of TOF-LIMS analyses showing profile plots of count ratios vs relative depth from the surface of the grains. Each individual plot represents analyses of 15 carbonate-mineral grains. Several siderite grains are included in the analyses from location A, the analyses from locations B to E represent the surfaces of ankerite grains. For each element, a separate profile plot is presented for each zone (A to E) within the tailings stratigraphy. The grain sample locations for this study, are shown at the left margin.

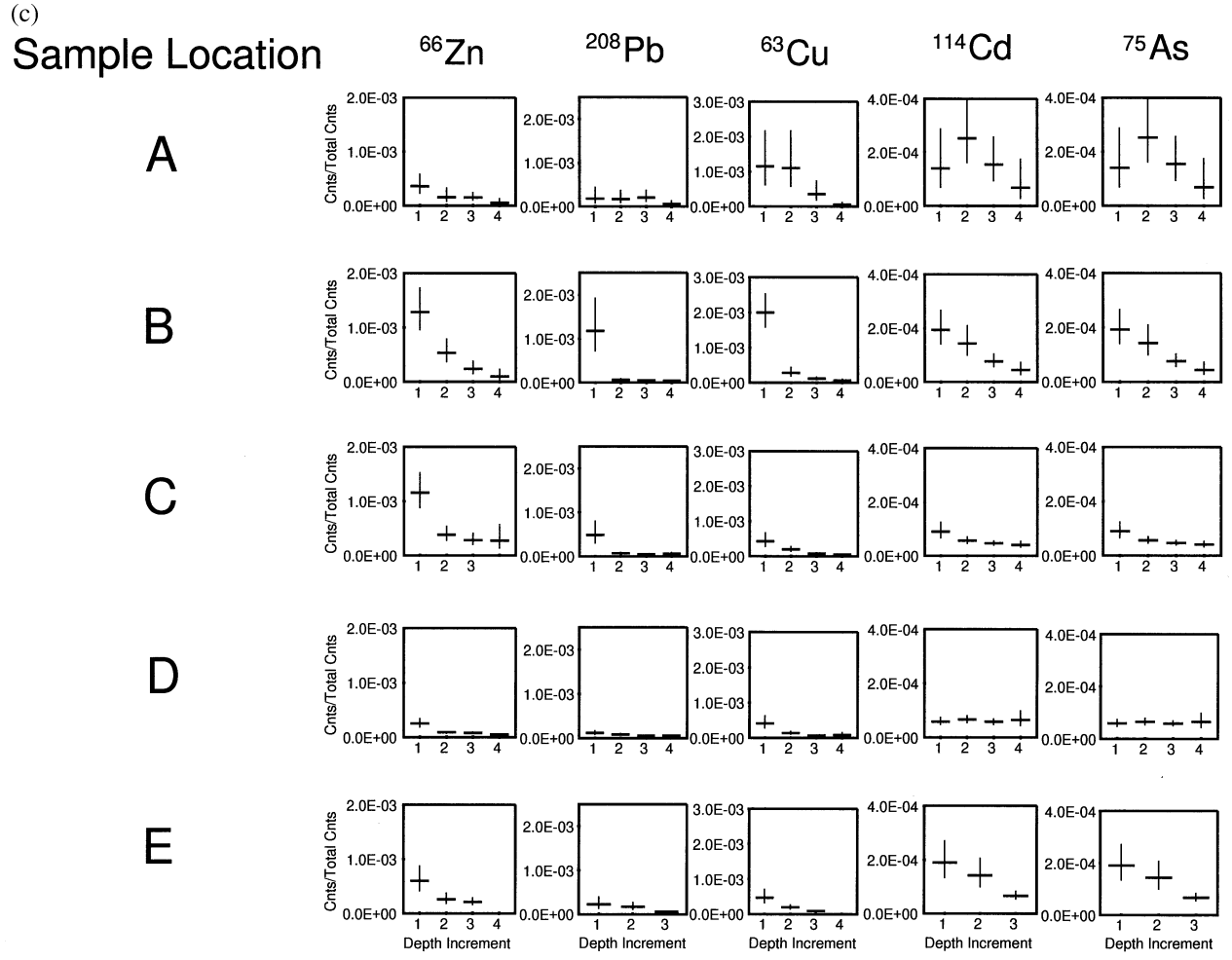

Fig. 4. Continued

The data can not be equated to elemental concentrations because, for a constant elemental concentration at the particle surface, the count ratio may vary according to changes in concentrations and ionization yields for other elements. The count-ratio profiles for each element in Figure 4 are presented for the five zones within the tailings section. The horizontal lines in the profiles represent the mean of the count ratios at each depth increment (n = 75), and the vertical lines represent the 95% confidence interval for the mean.

5.2.1. Major component cations (Ca, Mg, Fe, Mn)

When the TOF-LIMS analyses are considered collectively, a strong correlation is evident between the abundances of Ca and Fe (Fig. 6a). There are no similar correlations observed between the other major cation pairs (Fig. 6b,c). Within the trend displayed in Figure 6a, the low-Ca data points generally correspond to the surface of the carbonate grains, and the high-Ca data points correspond to the subsurface. Variations in the relative abundances with respect to depth from the grain surface are more easily observed when the data from the four depth increments are viewed separately. Throughout the entire thickness of tailings, the abundances of Ca and Mg are consistently lowest at the grain surfaces, and abundances increase toward the subsurface (Fig. 4). In contrast, the relative abundance of Fe is generally greatest near the surface of the grains, and decreases inward from the surface. Unlike Ca, Fe and Mg, the relative abundance of Mn does not display a systematic trend versus depth from the surface.

5.2.2. Trace-element components of carbonate minerals

Without exception, the relative abundances of the trace components (Al, As, Cd, Cu, K, Na, Pb, S, Zn) are highest near the surface of the mineral grains, and decrease inward from the grain surface. At the mineral surfaces, the abundances of all of these elements are lowest in the deep tailings below the natrojarosite-containing zone. The maximum abundances of As, Al, Cd, K and Na occur in the upper sulfide-oxidation zone, and the maximum abundances of Cu, Pb, S and Zn occur slightly deeper in the lower sulfide-oxidation zone, or in the natrojarosite-containing zone.

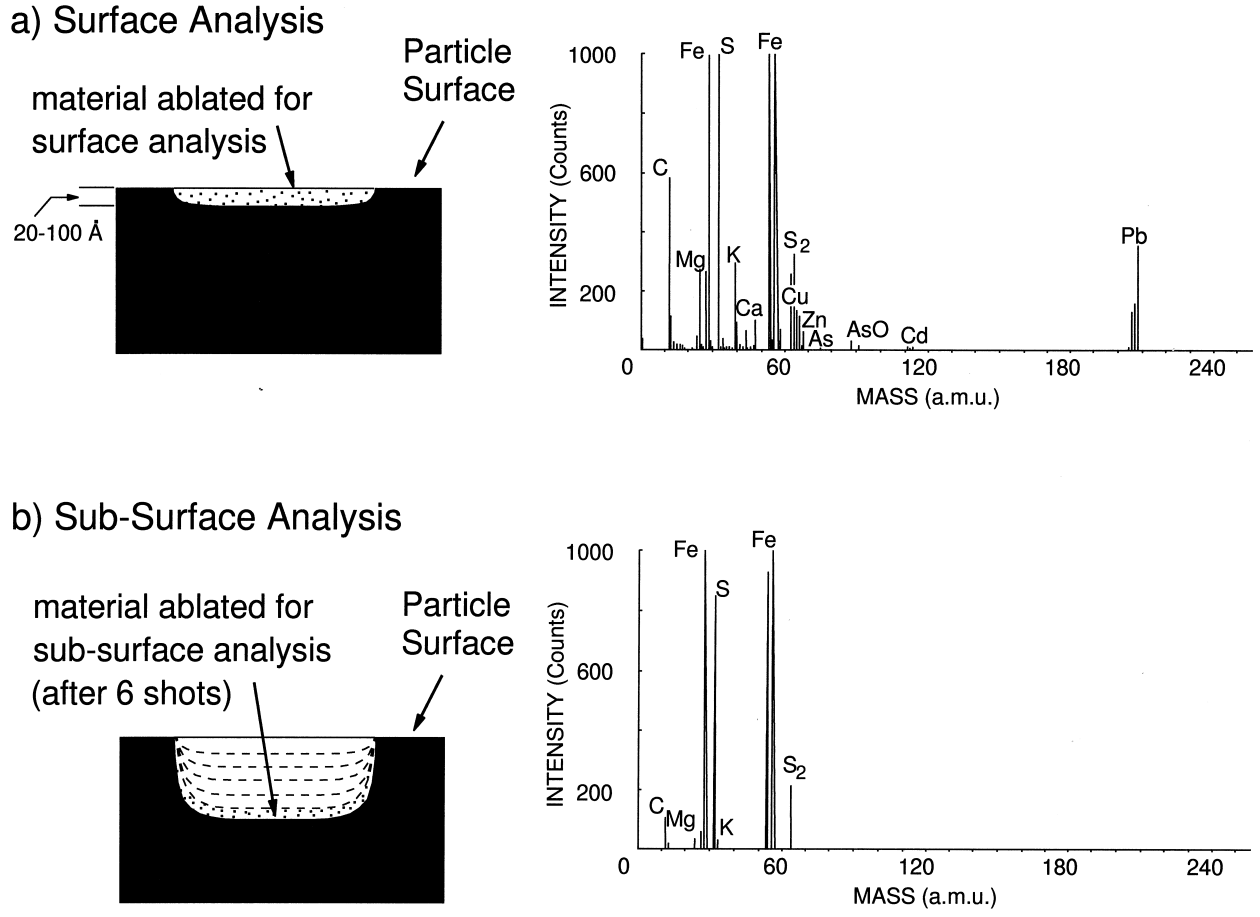

Fig. 5. Representative mass-resolved spectra for the average of 75 analyses of pyrite at a) the surface, and b) depth increment number four, in the natrojarosite-containing zone. Mass interferences from cluster ions are evaluated by monitoring the intensity of all isotopes. For example, note that the relative intensities for ^{204}Pb, ^{206}Pb, ^{207}Pb and ^{208}Pb are consistent with the relative isotopic abundances 1.4%, 24.1%, 22.1% and 52.4%, respectively. The intensity of ^{56}Fe is off scale in both a) and b).

Table 1. Pore-water chemical composition (mg/L) at the sample locations for carbonate grains.

Sample zone	A	B	C	D	E
Depth (m)	0.05	0.15	0.45	4.00	8.00
pH	3.85	4.36	6.76	6.55	6.98
E_H (mV)	621	621	217	94	165
HCO_3	—	—	12.2	190	48.0
Ca	452	458	440	369	451
Mg	3,000	3,550	1,780	317	175
Na	68.6	110	720	1,460	105
K	40.4	70.5	86.3	67.1	22.4
Si	28.2	40	21.3	9.5	3.4
Fe	19.4	0.7	254	388	7.7
Zn	1,430	4,080	421	0.65	0.15
Pb	1.08	2.29	0.27	0.2	—
Cu	2.61	1.68	0.07	—	—
Ni	6.61	7.62	1.08	0.06	—
Cd	42.8	53.6	0.79	—	—
Mn	887	811	86.6	2.67	1.25
As	0.021	—	0.045	0.019	0.023
Al	5.5	—	—	—	—
SO_4	21,400	22,900	10,080	5,580	3,740
Cl	16.3	28.4	54.0	16.0	16.2

5.3. Mineral Surfaces: Coating Mineralogy

Carbonate-mineral grains from the five geochemical zones within the tailings have been studied using TEM. Secondary mineral coatings were observed on almost all of the grains, except for a few siderite grains that were collected from the upper sulfide-oxidation zone. Coatings on the grains from this zone were generally thin and discontinuous around the margin of the primary carbonate mineral. In the deeper zones within the tailings, the coatings were observed to be up to 1000 nm thick. Most of the coatings are visible in cross section as fine-grained layers between the coarsely crystalline primary carbonate substrate and the surrounding resin (Figs. 7a,c and 8b,c). In rare cases in which the initial cut into the sample was preserved during microtoming, sections of the coatings were obtained tangential to the primary mineral surface (Figs. 7b, 8a, 9a). The cross-sectional images indicate that the coatings occur around the perimeter of the mineral grains, but it is clear from images obtained from the tangential sections (Fig. 9a) that fractures and cleavage planes are important controls on the alteration processes.

Table 2. Saturation indices[a] calculated from the tailings pore-water analytical data at the sample locations that correspond to the locations of the carbonate grains.

Sample location		A	B	C	D	E
Amorphous	$Al(OH)_3$	−5.87	—	—	—	—
[b]Spertiniite	$Cu(OH)_2$	−6.61	−5.76	−2.37	—	—
Theophrastite	$Ni(OH)_2$	−7.11	−5.94	−1.86	−3.26	—
[b]Amorphous	$Fe(OH)_3$	−0.18	−0.18	2.82	0.17	1.06
[b]Goethite	FeO(OH)	5.32	5.31	8.27	5.47	6.23
[b]Jarosite	$KFe_3(SO_4)_2(OH)_6$	4.46	2.96	4.56	−3.25	−2.69
[b]Natrojarosite	$NaFe_3(SO_4)_2(OH)_6$	0.92	−0.63	1.67	−5.8	−5.95
[b]Hydronium Jarosite	$(H_3O)Fe_3(SO_4)_2(OH)_6$	−0.63	−2.93	−3.91	−11.69	−11.31
[b]Melanterite	$FeSO_4 \cdot 7H_2O$	−3.72	−5.34	−2.54	−2.3	−3.92
Anglesite	$PbSO_4$	−0.4	−0.06	−1.01	−1.24	—
Gypsum	$CaSO_4 \cdot 2H_2O$	0.15	0.11	0.04	−0.03	0.07
Calcite	$CaCO_3$	—	—	−1.93	−0.99	−0.94
Dolomite	$(Ca,Mg)(CO_3)_2$	—	—	−3.04	−1.9	−2.21
Magnesite	$MgCO_3$	—	—	−1.65	−1.43	−1.77
Epsomite	$MgSO_4 \cdot 7H_2O$	−1.16	−1.13	−1.46	−2.17	−2.38
[b]Siderite	$FeCO_3$	—	—	−0.42	0.74	−1.02
Rhodochrosite	$MnCO_3$	—	—	−0.83	−1.32	−1.68
Smithsonite	$ZnCO_3$	—	—	−0.85	−2.67	−3.35
Cerussite	$PbCO_3$	—	—	−1.4	−0.57	—
Gaspeite	$NiCO_3$	—	—	−6.64	−7.08	—
Otavite	$CdCO_3$	—	—	−1.69	—	—
[b]Scorodite	$FeAsO_4 \cdot 2H_2O$	−1.04	—	−1.15	—	—

[a] Saturation indices have been calculated with the equilibrium geochemical model MINTEQA2 (Allison et al., 1991) using the WATEQ4F database from Ball and Nordstrom (1991).

[b] Activities of redox couples ($Fe^{II/III}$ and $Cu^{I/II}$) are calculated using E_H measurements and total concentrations. E_H measurement error increases with pH due to decreasing activity of $Fe^{(III)}$, therefore a lower level of confidence is attributed to these saturation indices in zones C to E.

Energy dispersive X-ray spectroscopy (EDS) results indicate that the chemical compositions of the coatings are variable. The composition of the coatings is generally dominated by Fe, with lesser amounts of Si, Ca, Al, Mg, Mn, S, Cl, Cu and Zn (in order of decreasing abundance). The two EDS spectra presented in Figure 10 are representative of analyses obtained from numerous locations within the tailings profile. The spectra, however, are not diagnostic of the coating mineralogy; electron diffraction patterns for various Fe oxyhydroxides and siderite have been acquired from coatings that display similar EDS analytical results.

Using SAED and CBED, goethite, akaganéite and siderite are the only minerals that could be identified with confidence as present in the coatings. On the basis of results from EDS analysis and electron-diffraction patterns, a phase interpreted to be amorphous ferric oxyhydroxides, perhaps ferrihydrite, was identified on carbonate-mineral grains from all zones within the tailings (Figs. 7c, 8c). Similarly, goethite was identified in all locations except the upper sulfide-oxidation zone. The thin, discontinuous nature of the coatings from the upper sulfide-oxidation zone precluded positive identification of the coating. Akaganéite was identified only in one sample collected from the mill-discharge water zone (Fig. 9b). Siderite coatings were identified on several ankerite grains, but only in the lower sulfide-oxidation zone and in the natrojarosite-containing zone (Figs. 7a,b and 8a,b). Invariably, the grain size of the siderite is finer than that of the primary ankerite substrate, and in one sample the siderite displays a dendritic habit (Fig. 8a).

6. DISCUSSION

6.1. Pore-Water Geochemistry

In the deep tailings, the pore-water composition is similar to that of the mill water that is discharged with the tailings. This observation suggests that there has been very little change in the pore-water composition in this zone since the tailings were deposited, and that the solid phases present within these tailings are relatively stable. The increased Na, K, Zn, Pb, As, HCO_3 and SO_4 concentrations in the pore water at intermediate depths within the tailings may be explained by the dissolution of natrojarosite (Al et al. 1994a). Increased concentrations of Zn and As also may be due to retention of Zn and As in the aqueous phase of the natrojarosite residue during co-disposal (Jambor and Owens, 1992). At neutral pH, natrojarosite dissolution is an acid-generating reaction, and the increased concentrations of Mg, Mn, Si and HCO_3 within this interval may be the result of carbonate- and alumino-silicate-mineral dissolution following natrojarosite dissolution (Al et al. 1994a). Near the surface of the tailings, Fe, Zn, Pb, Cu, Cd, Co, Ni, Cr and SO_4 are released to the pore water by oxidative dissolution of sulfide minerals. The increased concentrations of Fe, Mg, Mn, Si and Al in the pore water near the surface are related to acid-neutralization reactions involving carbonate and alumino-silicate minerals.

6.2. Reactions at Carbonate-Mineral Surfaces

The compositional data obtained from TOF-LIMS analysis are used with images, EDS analyses and electron-diffraction

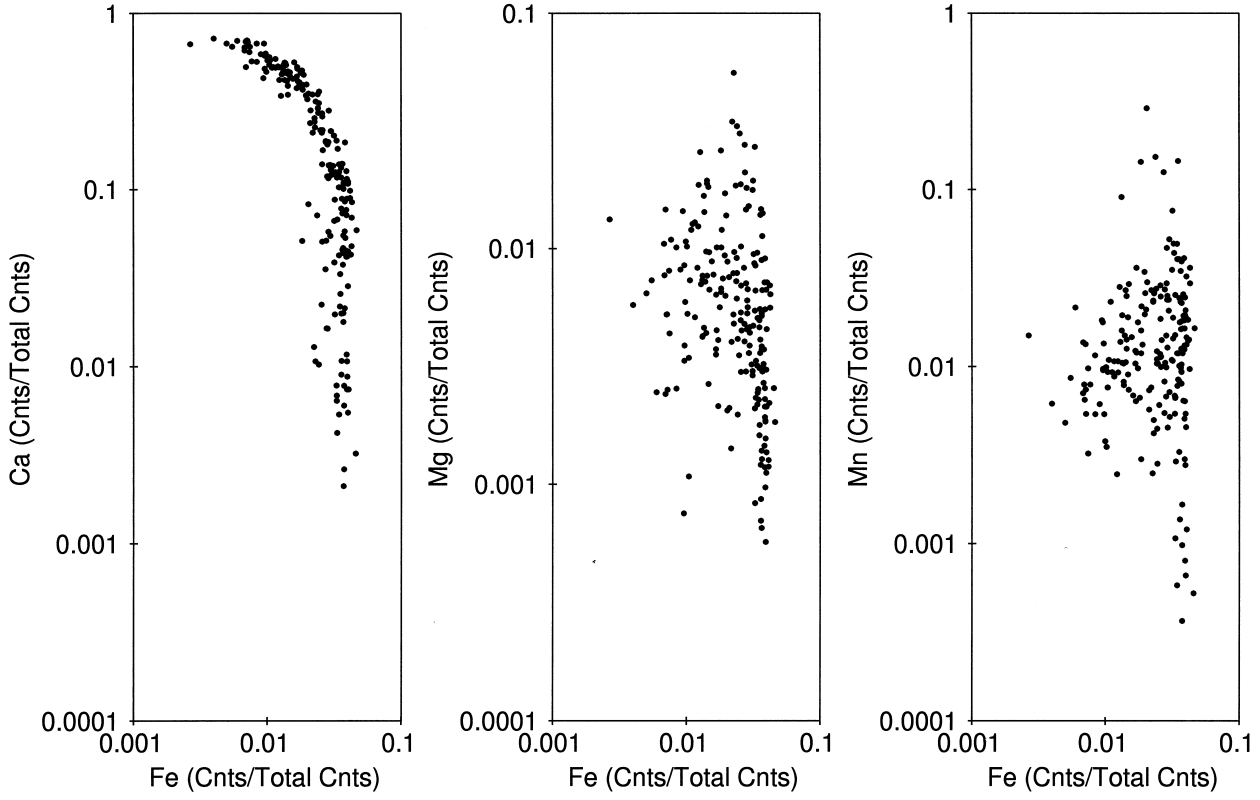

Fig. 6. Abundances of a) Ca vs. Fe, b) Mg vs Fe and c) Mn vs Fe, obtained by TOF-LIMS analysis at the surface, and at three depth increments below the surface of the carbonate minerals collected from the five geochemical zones within the tailings.

data obtained with the TEM, to make inferences regarding the reactions that occur at the mineral surface. The TOF-LIMS data provide a qualitative assessment of the composition of surface coatings. Presentation of the data as count ratios provides a relative measure of the abundance of specific elements in the material removed from the surface by the ablation laser, and ionized by the post-ablation laser. The sampling volume for the ablation laser is not constant for different samples, and the mass removed and ionized is not known. Therefore the data can not be considered in terms of concentrations of the elements in the surface coatings. The same limitations exist for successive analyses at the same location, and variations in relative abundances in depth profiles are not quantitative.

Determination of the mineralogy of surface coatings by TEM may be affected by phase transformations during sample preparation or electron beam impingement. These effects are of particular concern for samples that have been obtained from anoxic groundwater systems, as exposure to atmospheric oxygen during the mineral separation procedures is likely to cause oxidation of redox-sensitive minerals. Thus, we can not be certain that commonly observed minerals such as goethite, are not products of the oxidation of less stable precursors, such as ferrihydrite.

6.2.1. Major Cations (Ca, Mg, Fe, Mn)

The observed correlation between Ca and Fe abundances (Fig. 6a) is suggestive of stoichiometric replacement of Ca by Fe toward the surface of the carbonate minerals. Incongruent dissolution of ankerite is a plausible explanation for the correlation between the abundances of Ca and Fe, as well as the apparent depletion of Ca and Mg nearest the surface. Under the influence of a long-term infiltration flux of acidity from sulfide oxidation near the tailings surface, carbonate minerals, including ankerite, will dissolve gradually. Secondary-mineral coatings at the ankerite surface represent a barrier to mass transport, creating conditions in which the pore water is undersaturated with respect to both ankerite and calcite. Based on differences in the solubility of the respective carbonate minerals, and because Ca has only a limited solid solution with siderite, magnesite or rhodochrosite, Ca from ankerite dissolution is more likely than Fe, Mg and Mn to remain in the aqueous phase. Some of the Ca released through dissolution of ankerite may be retained at the surface by precipitation of gypsum, as is suggested by gypsum saturation indices (Table 2) and by the high relative abundance of S near the carbonate-mineral surfaces (Fig. 4). Al et al. (1997) suggested that gypsum precipitates were responsible for elevated abundances of Ca on the surface of pyrite grains collected from the same cores that were the source of the carbonate grains for this study.

Under anoxic conditions, Fe, Mg and Mn may re-precipitate at the ankerite surface as siderite, magnesite, rhodochrosite, or a solid solution of these components. This inferred mechanism is supported by commonly observed positive saturation indices for siderite in tailings pore water (Dubrovsky et al., 1985;

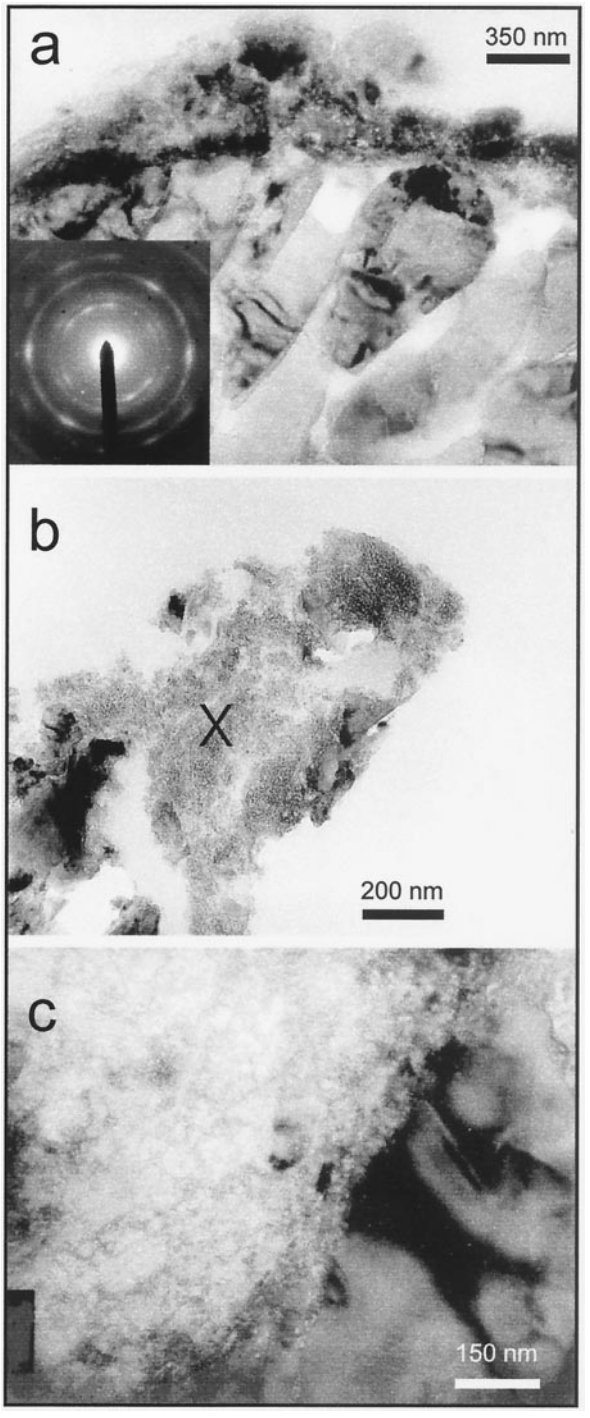

Fig. 7. TEM images of secondary-mineral coatings at the surface of ankerite from the lower sulfide-oxidation zone. a) The secondary-mineral coating (left to right in the upper portion of the image) in contact with coarse crystalline ankerite (lower portion of image) is identified as siderite using EDS and SAED (inset). b) Section cut tangential to the ankerite surface through a secondary-mineral coating (light area), and a protruding portion of the ankerite grain (dark area in lower left). The secondary mineral is identified as siderite using EDS and CBED. c) Secondary-mineral coating (light area at left) identified as amorphous Fe oxyhydroxide by EDS and by the absence of crystallinity in an electron diffraction pattern.

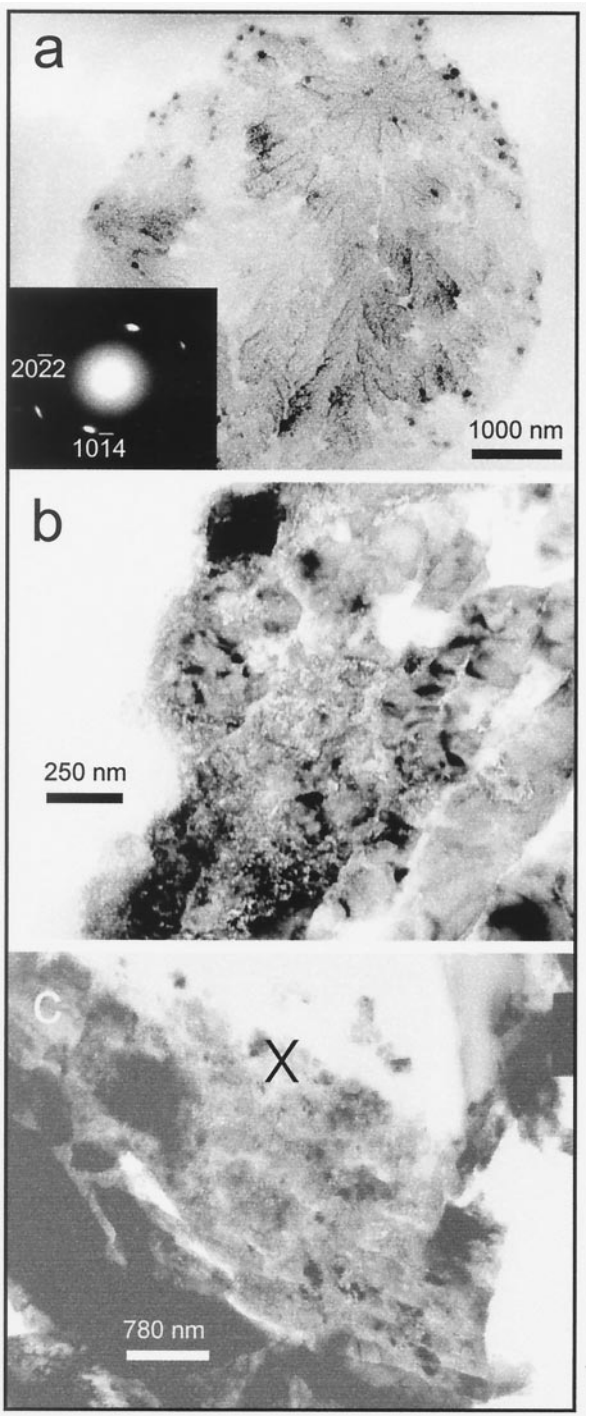

Fig. 8. TEM images of secondary-mineral coatings at the surface of ankerite from the natrojarosite-containing zone. a) Section cut tangential to the ankerite surface through a secondary-mineral coating displaying a dendritic crystal-growth pattern. The secondary mineral is identified as siderite using EDS and SAED (inset). b) The secondary-mineral coating (slightly darker grey and fine grained from top to bottom in the central portion of the image) in contact with coarse crystalline ankerite (right side of the image) is identified as siderite using EDS and SAED. c) Secondary-mineral coating (light area in center of the image) identified as amorphous Fe oxyhydroxide by EDS and by the absence of crystallinity in an electron diffraction pattern.

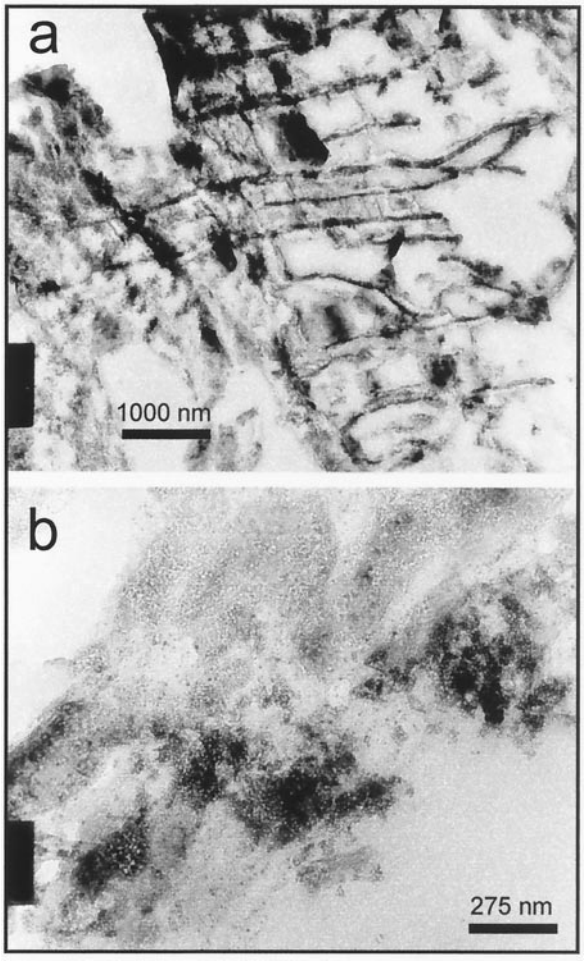

Fig. 9. TEM images of secondary-mineral coatings at the surface of ankerite from the mill discharge-water zone. a) Image at low magnification of a section cut tangential to the ankerite surface shows the occurrence of secondary minerals along traces of fractures and cleavage planes. b) Secondary-mineral coating (light mottled area in upper portion of the image) identified as akaganéite based on EDS and CBED.

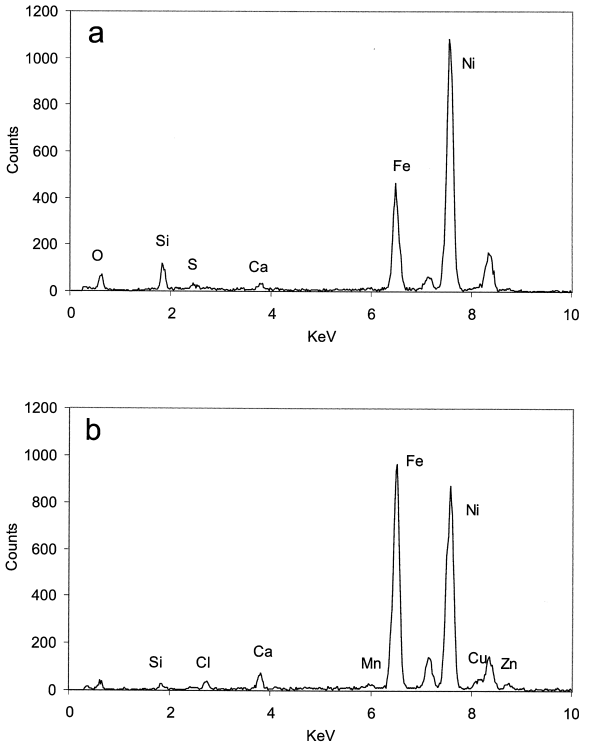

Fig. 10. Typical EDS spectra for secondary-mineral coatings on ankerite. a) EDS spectrum obtained from the coating shown in Figure 7c. Based on the EDS analysis, and the inability to obtain an electron diffraction pattern, this material was identified as amorphous ferric oxyhydroxide. b) EDS spectrum obtained from the coating shown in Figure 7b. The EDS analysis and electron-diffraction patterns were used to identify this material as siderite. The large Ni peaks are from the Ni-wire grid used to support the sample in the TEM.

Morin and Cherry, 1986; Al et al., 1994a; Blowes and Ptacek, 1994), and by the identification of siderite at the surface of ankerite (Figs. 7a,b and 8a,b). Under oxic conditions, the $Fe^{(II)}$ that is released by ankerite dissolution is likely to oxidize to $Fe^{(III)}$ and form ferric oxyhydroxide coatings on the ankerite surface. In addition to siderite, TEM investigations have confirmed the presence of a variety of ferric oxyhydroxide coatings on the ankerite surfaces (Figs. 7c and 8c). Under oxic conditions, the Mg and Mn that are released by ankerite dissolution may either precipitate as magnesite and rhodochrosite if the pore-water pH is suitably high, or remain in the aqueous phase. Precipitation of Mn-oxides is not expected because of the slow kinetics of $Mn^{(II)}$ oxidation at neutral and lower pH. Based on the conceptual model presented above, the observed correlation between Ca and Fe is expected because in either oxic or anoxic conditions it is possible to deplete Ca near the surface by dissolving ankerite, and the Fe from ankerite will remain immobile as a secondary coating. No similar correlation is observed between the other cation pairs because the Mg and Mn components of the ankerite solid-solution are variable, and because the partitioning of Mg and Mn between the pore water and the mineral surfaces varies depending on pH and redox conditions.

Equilibrium geochemical modeling (PHREEQC, Parkhurst, 1995) was used to test this conceptual model under anoxic conditions. Simulations under oxic conditions were not conducted because the kinetic limitations on $Fe^{(II)}$ and $Mn^{(II)}$ oxidation are not accounted for by the computer model. The geochemical conditions measured in the tailings pore water in the natrojarosite-containing zone (Table 1) were used as the initial conditions for the simulations. Ankerite [$Ca(Fe_{0.6}Mg_{0.4})(CO_3)_2$] was added to the thermodynamic database that was used for the simulations (Wateq4f; Ball and Nordstrom, 1991). The solubility product for ankerite ($\text{Log } K = -17.40$) was calculated assuming ideal solid-solution mixing, using ΔG_f^o data for ions and $CaMg(CO_3)_2$ from Robie et al. (1979), and for $CaFe(CO_3)_2$ from Wogelius et al. (1992). It was assumed that ankerite was present in excess, and that the pore water was undersaturated with respect to ankerite ($SI = -3.0$) due to the formation of secondary-mineral coatings. Calcite, magnesite, siderite, rhodochrosite and gypsum were allowed to precipitate if the saturation index for these phases exceeded 0.0. A stepwise reaction was simulated such that for every mole of reaction added (Fig. 11), 2.0 moles of H^+, 2.0 moles of SO_4, and

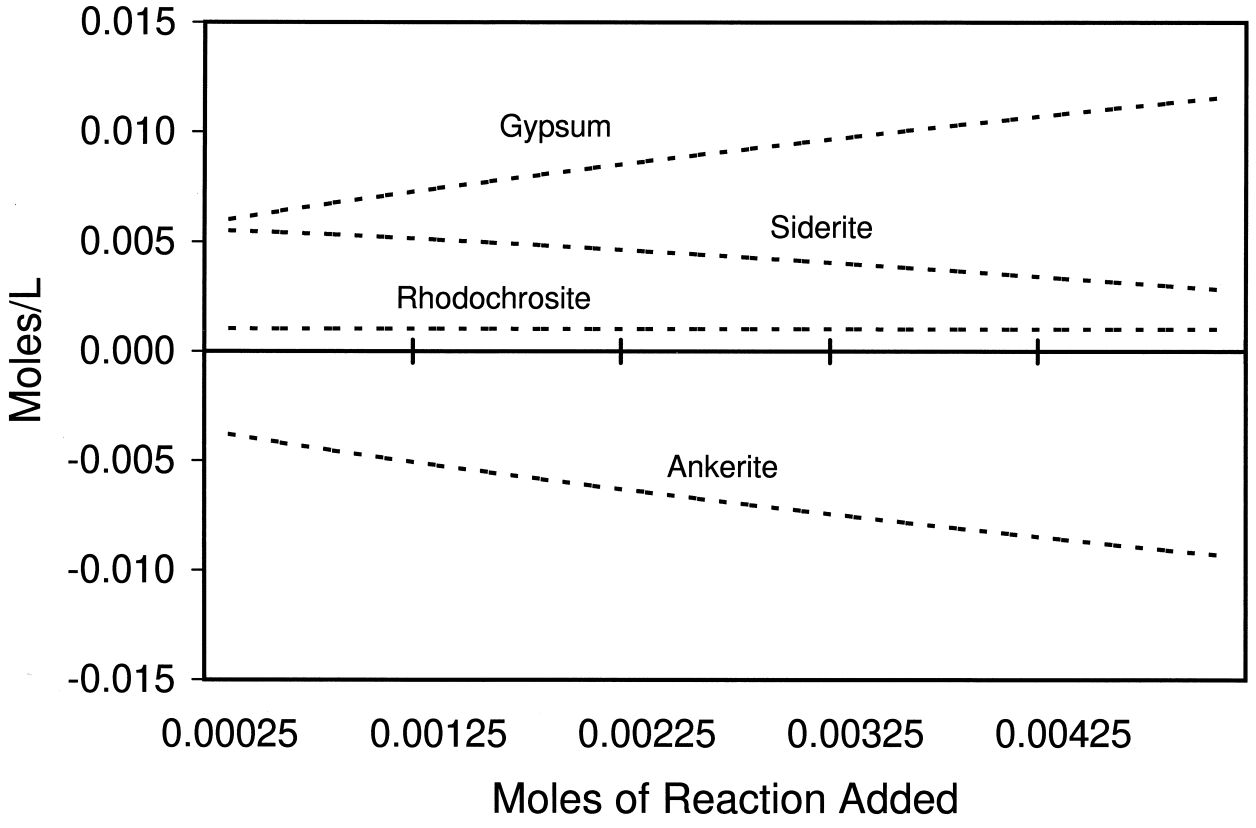

Fig. 11. Results of simulated reactions between ankerite and hypothetical solutions containing variable amounts of H^+, SO_4 and Fe. Ankerite is present in excess, and the $SI_{ankerite}$ is maintained at -3.0 to emulate a transport-limited kinetic limitation to ankerite dissolution. Positive values indicate mineral precipitation (siderite and gypsum) and negative values indicate dissolution (ankerite). The predicted precipitation of siderite and gypsum is consistent with observations from mineralogical investigations of the Kidd Creek tailings.

0.25 moles of Fe were added to the model system. This stoichiometry is representative of pyrite oxidation except that a further assumption was made that 75% of the Fe released by pyrite oxidation does not infiltrate to depth within the tailings, and is attenuated by the formation of Fe oxyhydroxide minerals in the oxic zone of the tailings.

The results of the simulations suggest that the conceptual model is thermodynamically viable. The non-equilibrium dissolution of ankerite is accompanied by precipitation of siderite, rhodochrosite, and gypsum (Fig. 11). The pore water remains undersaturated with respect to calcite and magnesite throughout the simulations.

6.2.2. Trace-element components of carbonate minerals

Geochemical modeling suggests that the pore water in the sulfide-oxidation zone (A and B) is saturated to supersaturated with respect to jarosite and natrojarosite (Table 2). Jarosite is a common secondary mineral in oxidized, sulfide-rich tailings (Jambor, 1994). The pore-water concentrations of Na and K near the surface of the tailings consistently decreased between 1992 (527 mg/L Na; 93.8 mg/L K), 1993 (170 mg/L Na; 84.4 mg/L K) and 1994 (68.6 mg/L Na; 40.4 mg/L K). Assuming equilibrium between the infiltrating pore water and the natrojarosite that was co-disposed with the tailings, it is expected that precipitation of secondary jarosite-type minerals, and decreasing K and Na concentrations, would occur as the activity of SO_4 increases due to sulfide oxidation. The geochemical modeling results, the gradual decrease in Na and K concentrations, and the abundance of Na, K, Fe and S on the carbonate surfaces (Fig. 4) in these zones are consistent with precipitation of secondary coatings of Na-K jarosite on the carbonate grains.

The high relative abundance of Al on carbonate surfaces in the low-pH, sulfide-oxidation zone (Fig. 4) is consistent with the low pK_1 of Al^{3+}, which is lower than for many other cations, resulting in more extensive hydrolysis and greater potential for Al adsorption at low pH. The high relative abundance of Al on the surfaces in this zone also may result from co-precipitation of Al with a ferric oxyhydroxide mineral, as has been observed previously in laboratory studies (Fitzpatrick and Schwertmann, 1982; Taylor et al., 1990; Gerth, 1990).

The pore-water concentrations of Zn, and Pb are high in the upper sulfide-oxidation zone (Table 1) as a result of oxidative dissolution of metal-bearing sulfide minerals. Despite the high aqueous concentrations of metals in this zone, their relative abundances on carbonate surfaces are very low (Fig. 4). With increasing depth below the sulfide-oxidation zone, the aqueous concentrations of these elements decrease, their relative abundance on carbonate surfaces increases, and these changes co-

incide with a sharp increase in pH (4.36 to 6.76). Similar trends versus pH in the abundance of metals on the surface of soil and mine tailings grains were noted by Tingle et al. (1993) and Al et al. (1997). These trends are consistent with a cation adsorption mechanism for attenuation of the metals on the surface of the grains. There are no indications from the geochemical modeling or TEM studies that precipitation of a discrete secondary phase has occurred, thereby attenuating the concentrations.

In contrast with Pb and Zn, the abundance of Cu and Cd at the carbonate-mineral surfaces is high in the low-pH upper sulfide-oxidation zone (Fig. 4). Otherwise, the distribution of Cu and Cd in the pore water and at the surface of the carbonate-mineral grains is similar to the distribution of Pb and Zn. Adsorption of these metals is not favored at low pH, suggesting that the attenuation of Cu and Cd at the mineral surfaces is controlled by precipitation or co-precipitation within a secondary-mineral coating.

Geochemical modeling of pore-water speciation indicates that the dominant As species are the hydrolysis products of arsenate ($HAsO_4^{2-} = H_2AsO_4^- > H_3AsO_4^o$). This speciation was not confirmed analytically. The surface charge on the carbonate minerals or secondary-mineral coatings in the low-pH sulfide-oxidation zone is greater than at neutral or high pH. Under these conditions, adsorption of anionic arsenic species released to the pore water through oxidative dissolution of As-bearing sulfide minerals and dissolution of natrojarosite would be favored (Pierce and Moore, 1982; Dzombak and Morel, 1990). Based on calculated saturation indices (Table 2), the attenuation of As concentrations in the pore water through precipitation of scorodite is not a likely explanation for increased abundance of As on the mineral surfaces. Adsorption and co-precipitation of As with minerals common to mine-tailings such as jarosite and ferrihydrite have been well documented (Dutrizac and Jambor, 1987; Waychunas et al., 1993; Fuller et al., 1993), and these mechanisms represent the most likely explanation for the increased abundance of As on the surface of carbonate grains (Fig. 4).

The detection of S at the surface of the carbonate minerals (Fig. 4) reflects the presence of SO_4, as SO_4 is the stable S species in the oxidized tailings system. The abundance of S at the mineral surfaces is greatest in the upper and lower sulfide-oxidation zone, coinciding with the highest aqueous concentrations of SO_4 (Table 1). The pore water in the upper and lower sulfide-oxidation zones is slightly supersaturated with respect to gypsum, jarosite and natrojarosite, and precipitation at the surface of the carbonate minerals probably accounts for the increased abundance of S on the mineral surfaces in these zones.

7. CONCLUSIONS

Coatings of secondary minerals have been observed on almost all of the carbonate-mineral grains that were recovered from the tailings, and it is likely that most of the primary minerals (carbonates, sulfides, alumino-silicates and oxides) in tailings and waste-rock systems are affected similarly. With regard to research efforts to numerically simulate reactive-solute transport in tailings and waste-rock groundwater systems (Narasimhan et al., 1986; Morin and Cherry, 1988; Walter et al., 1994a;b; Wunderly et al., 1995; 1996; Mayer 1998), there are several important implications of the presence of such coatings. The accumulation of coatings will diminish the rates of mass transfer between primary minerals and the pore water, thereby reducing the rate of mineral-precipitation and dissolution reactions involving the primary minerals. The reduction in the rates will be a function of time as the coatings accumulate gradually. Consequently, the use of kinetic rate constants obtained from the literature for modeling precipitation and dissolution of mineral phases will likely overestimate the actual rates. Our data suggest that conceptual and numerical models for reactive transport in mine-waste systems could be improved by incorporating incongruent dissolution processes, coupled with lower dissolution reaction rates for dolomite and ankerite than are obtained from most kinetic studies. This also may be true for the dissolution of many alumino-silicate minerals that are known to dissolve incongruently (Langmuir, 1997).

The TOF-LIMS data indicate that adsorption, surface-complexation and co-precipitation reactions are important controls on the concentrations of trace elements in the pore water. The occurrence of coatings of secondary minerals on primary minerals is widespread, and reactions with the secondary minerals, rather than the primary mineral substrate, probably represent the principal controls on the trace-element distribution in the pore water. Conceptual and numerical models for reactive transport of trace metals in these systems will benefit from additional research aimed at identifying the important secondary minerals, and the mineralogical, thermodynamic and kinetic constraints on trace-element partitioning to these minerals.

Acknowledgments—Falconbridge Limited, Kidd Creek Division, provided funding for the tailings pore-water geochemistry portion of this study. The TOF-LIMS analyses were funded by the Applied Mineralogy Program (CANMET/MMSL). TOF-LIMS analyses were conducted at the Advanced Mineral Technology Laboratory (AMTEL) in London, Ontario. The TEM investigations were funded by the Natural Science and Engineering Research Council (NSERC), through a research grant to T. Al. Susan Belfry (Electron Microscopy Unit-UNB) provided valuable assistance in preparing samples for TEM. Comments provided by J. L. Jambor and two anonymous reviewers helped to improve the paper.

Special handling: J. D. Rimstidt

REFERENCES

Al T. A. and Blowes D. W. (1996) Storm-water hydrograph separation of run off from a mine-tailings impoundment formed by thickened tailings discharge at Kidd Creek, Timmins, Ontario. *J. Hydrol.* **180(1–4),** 55–78.

Al T. A. and Blowes D. W. (1999) The hydrogeology of a tailings impoundment formed by central discharge of thickened tailings: implications for tailings management. *J. Cont. Hydrol.* **38,** 489–505.

Al T. A., Blowes D. W., Jambor J. L., and Scott J. D. (1994a) The geochemistry of mine-waste pore water affected by the combined disposal of natrojarosite and base-metal sulphide tailings at Kidd Creek, Timmins, Ontario. *Can. Geotech. J.* **31,** 502–512.

Al T. A., Blowes D. W., and Jambor J. L. (1994b) A geochemical study of the main tailings impoundment at the Falconbridge Limited, Kidd Creek Division Metallurgical Site, Timmins, Ontario. In *Environmental Geochemistry of Sulfide Mine-Wastes* (eds. J. L. Jambor and D. W. Blowes), Mineralogical Association of Canada Short Course, **22,** 333–364.

Al T. A., Blowes D. W., Martin, C. J., Cabri, L. J., and Jambor J. L. (1997) Aqueous geochemistry and analysis of pyrite surfaces in

sulfide-rich mine tailings. *Geochim. Cosmochim. Acta* **61,** 2353–2366.

Allison J. D., Brown D. S., and Novo-Gradac K. J. (1991) *MINTEQA2/PRODEFA2, A Geochemical Assessment Model for Environmental Systems: Version 3.0 User's Manual.* United States Environmental Protection Agency, Athens GA. US/EPA/600/3–91/021.

Ball J. W. and Nordstrom D. K. (1991) *Users Manual for WATEQ4F with Revised Thermodynamic Database and Test Cases for Calculating Speciation of Major, Trace and Redox Elements in Natural Waters.* USGS open-file report 91-183.

Blowes D. W. and Ptacek C. J. (1994) Acid-neutralization mechanisms in inactive mine tailings. In *Environmental Geochemistry of Sulfide Mine-Wastes* (eds. J. L. Jambor and D. W. Blowes), Mineralogical Association of Canada Short Course, **22,** 271–292.

Blowes D. W., Reardon E. J., Jambor J. L., and Cherry J. A. (1991) The formation and potential importance of cemented layers in inactive sulfide mine tailings. *Geochim. Cosmochim. Acta* **55,** 965–978.

Booth J., Hong Q., Compton R. G., Prout K., and Payne R. M. (1997) Gypsum overgrowths passivate calcite to acid attack. *J. Coll. Interf. Sci.* **192,** 207–214.

Brady P. V., Papenguth H. W. and Kelly J. W. (1999) Metal sorption to dolomite surfaces. *Appl. Geochem.* **14,** 569–579.

Bruno J., Duro L., de Pablo J., Casa I., Ayora C., Delgado J., Gimeno M.J., Peña Linklater C., Pérez del Villar L., and Gómez P. (1998) Estimation of the concentrations of trace metals in natural systems: The application of codissolution and coprecipitation approaches to El Berrocal (Spain) and Poços de Caldas (Brazil). *Chem. Geol.* **151,** 277–291.

Charlet L., Wersin P., and Stumm W. (1990) Surface charge of $MnCO_3$ and $FeCO_3$. *Geochim. Cosmochim. Acta* **54,** 2329–2336.

Cheng L., Lyman P. F., Sturchio N. C., and Bedzyk M. J. (1997) X-ray standing wave investigation of the surface structure of selenite anions adsorbed on calcite. *Surf. Sci.* **382,** L690–L695.

Chiarello R. P. and Sturchio N. C. (1994) Epitaxial growth of otavite on calcite observed in situ by synchrotron X-ray scattering. *Geochim. Cosmochim. Acta* **58,** 5633–5638.

Chiarello R. P., Sturchio N. C., Grace J. D., Geissbuhler P., Sorensen L. B., Cheng L. W., and Xu S. T. (1997) Otavite-calcite solid-solution formation at the calcite-water interface studied in-situ by synchrotron X-ray scattering. *Geochim. Cosmochim. Acta* **61,** 1467–1474.

Cravotta C. A. III, and Trahan M. K. (1999) Limestone drains to increase pH and remove issolved metals from acidic mine drainage. *Appl. Geochem.* **14,** 581–606.

Davis J. A., Fuller C. C., and Cook A. D. (1987) A model for trace metal sorption processes at the calcite surface: Adsorption of Cd^{2+} and subsequent solid solution formation. *Geochim. Cosmochim. Acta* **51,** 1477–1490.

Dietzel M. and Usdowski E. (1996) Coprecipitation of Ni^{2+}, Co^{2+} and Mn^{2+} with galena and covellite, and of Sr^{2+} with calcite during crystallization via diffusion of H_2S and CO_2 through polyethylene at 20 degrees C power-law and Nernst-Law control of trace-element partitioning. *Chem. Geol.* **131(1–4),** 55–65.

Dubrovsky N. M., Cherry J. A., Reardon E. J., and Vivyurka A. J. (1985) Geochemical evolution of inactive pyritic tailings in the Elliot Lake uranium district. *Can. Geotech. J.* **22,** 110–128.

Dutrizac, J. E. and Jambor, J. L. (1987) The behaviour of arsenic during jarosite precipitation: Arsenic Precipitation at 97°C from sulphate or chloride media. *Can. Metall. Quart.* **26,** 91–101.

Dzombak D. A. and Morel M. M. (1990) Surface Complexation Modelling. John Wiley & Sons, New York.

Fitzpatrick R. W. and Schwertmann U. (1982) Al-substituted goethite—An indicator of pedogenic and other weathering environments in South Africa. *Geoderma* **27,** 335–347.

Fuller C. C., Davis J. A., and Waychunas G. A. (1993) Surface chemistry of ferrihydrite: Part 2. Kinetics of arsenate adsorption and coprecipitation. *Geochim. Cosmochim. Acta* **57,** 2271–2282.

Gerth J. (1990) Unit-cell dimensions of pure and trace-metal associated goethites. *Geochim. Cosmochim. Acta* **54,** 363–371.

Jambor J. L. (1994) Mineralogy of sulfide-rich tailings and their oxidation products. In *Environmental Geochemistry of Sulfide Mine-Wastes* (eds. J. L. Jambor and D.W. Blowes), Mineralogical Association of Canada Short Course **22,** 59–102.

Jambor J. L. and Owens D. R. (1992) Mineralogical characterization of process products and secondary phases in the Kidd Creek jarosite impoundment, Timmins, Ontario. Division Rept. MSL 92–29 (CR). CANMET, Energy, Mines and Resources, Canada.

Jambor J. L., Owens D. R., Carrière P., and Lastra R. (1993) Mineralogical investigation of tailings and associated waste products, and the distribution of natrojarosite in the Kidd Creek main tailings cone, Timmins, Ontario. Division Rept. MSL 93-20 (CR). CANMET, Energy, Mines and Resources, Canada.

Jurjovec J., Blowes D. W., and Ptacek C. J. (1995) Acid neutralization in mill tailings and the effect of natrojarosite addition. *Proc. Sudbury '95, Mining and the Environment*, CANMET, Energy Mines and Resources, Canada, **1,** 29–38.

Langmuir D. (1997) Aqueous Environmental Geochemistry, Prentice-Hall, Inc., New Jersey.

Martin C. J., Al T. A., and Cabri L. J. (1997) Surface analysis of particles in mine tailings by TOF-LIMS. *Env. Geol.* **32(2), 107–113.**

Morin K. A. and Cherry J. A. (1986) Trace amounts of siderite near a uranium tailings impoundment, Elliot Lake, Ontario, Canada, and its implication in controlling contaminant migration in a sand aquifer. *Chem. Geol.* **56,** 117–134.

Morin K. A. and Cherry J. A. (1988) Migration of acid groundwater seepage from uranium tailings impoundments: 3. Simulation of the conceptual model with application to seepage area A. *J. Contam. Hydrol.* **2,** 323–342.

Mucci A. and Morse J. W. (1983) The incorporation of Mg^{2+} and Sr^{2+} into calcite overgrowths: Influences of growth rate and solution composition. *Geochim. Cosmochim. Acta* **47,** 217–233.

Narasimhan T. N., White A. F., and Tokunaga T. (1986) Groundwater contamination from an inactive uranium mine tailings pile: 2. Application of a dynamic mixing model. *Wat. Res. Res.* **22(3),** 1820–1834.

Odom R. W. and Schueler B. (1987) Thin film microanalysis using laser ablation and laser ionization mass spectrometry. *Thin Solid Films* **154,** 1–10.

Odom R. W. and Schueler B. (1990) Laser microprobe mass spectrometry: Ion and neutral analysis. In *Lasers and Mass Spectrometry*, (ed. D. M. Lubman), Oxford Series on Optical Sciences, Oxford University Press, New York, 103–137.

Parkhurst D. L. (1995) *User's Guide to PHREEQC—A Computer Program for Speciation, Reaction-Path, Advective-Transport, and Inverse Geochemical Calculations.* U.S. Geol. Survey, Water Resources Investigations Report 95–4227.

Pierce M. L. and Moore C. B. (1982) Adsorption of arsenite and arsenate on amorphous iron hydroxide. *Wat. Res. Res.* **16,** 1247–1253.

Rimstidt J. D., Balog A., and Webb J. (1998) Distribution of trace elements between carbonate minerals and aqueous solutions. *Geochim. Cosmochim. Acta* **62,** 1851–1863.

Robbins E. I., Cravotta C. A. III, Savela C. E., and Nord G. L. Jr. (1999) Hydrobiogeochemical interactions in >anoxic = limestone drains for neutralization of acidic mine drainage. *Fuel* **78,** 259–270.

Robie R. A., Hemingway B. S., and Fisher J. R. (1979) *Thermodynamic Properties of Minerals and Related Substances at 298.15 K and 1 Bar Pressure and at Higher Temperatures.* U.S. Geological Survey Bulletin 1452.

Stipp S. L. and Hochella M. F. Jr. (1991). Structure and bonding environments at the calcite surface as observed with X-ray photoelectron spectroscopy (XPS) and low energy electron diffraction. *Geochim. Cosmochim. Acta* **55,** 1723–1736.

Sturchio N. C., Chiarello R. P., Cheng L. W., Lyman P. F., Bedzyk M. J., Qian Y. L., You H. D., Yee D., Geissbuhler P., Sorensen L. B., Liang Y., and Baer D. R. (1997) Lead adsorption at the calcite-water interface—synchrotron X-ray standing wave and X-ray reflectivity studies. *Geochim. Cosmochim. Acta* **61,** 251–263.

Taylor R. M., Raupach M., and Chartres C. J. (1990) Simulation of soil reactions: Aluminum-iron(III) hydroxy species react with silica to give deposits on particle surfaces. *Clay Minerals.* **25,** 375–389.

Tesoriero A. J. and Pankow J. F. (1996) Solid-solution partitioning of Sr^{2+}, Ba^{2+}, and Cd^{2+} to calcite. *Geochim. Cosmochim. Acta* **60,** 1053–1063.

Tingle T. N., Borch R. S., Hochella M. F. Jr., Becker C. H., and Walker

W. J. (1993) Characterization of lead on mineral surfaces in soils contaminated by mining and smelting. *Appl. Surf. Sci.* **72,** 301–306.

Walter A. L., Frind E. O., Blowes D. W., Ptacek C. J. and Molson, J. W. (1994a) Modelling of multicomponent reactive transport in groundwater: 1. Model Development and Evaluation. *Wat. Res. Res.* **30(11),** 3137–3148.

Walter A. L., Frind E. O., Blowes D. W., Ptacek C. J., and Molson J. W. (1994b) Modelling of multicomponent reactive transport in groundwater: 2. Metal mobility in aquifers impacted by acidic mine tailings discharge. *Wat. Res. Res.* **30**(11), 3149–3158.

Wang Y. and Merino E. (1992) Dynamic model of oscillatory zoning of trace elements in calcite: Double layer, inhibition, and self-organization. *Geochim. Cosmochim. Acta* **56,** 587–596.

Waychunas G. A., Rea B. A., Fuller C. C., and Davis J. A. (1993) Surface chemistry of ferrihydrite: Part 1. EXAFS study of the geometry of coprecipitated and adsorbed arsenate. *Geochim. Cosmochim. Acta* **57,** 2251–2269.

Wogelius R. A., Fraser D. G., Feltham D. J., and Whiteman M. I. (1992) Trace element zoning in dolomite: Proton microprobe data and thermodynamic constraints on fluid composition. *Geochim. Cosmochim. Acta* **56,** 319–334.

Wunderly M., Blowes D. W., Frind E. O., Ptacek C. J., and Al T. A. (1995) A multicomponent reactive-transport model incorporating kinetically controlled pyrite oxidation. *Proc. Sudbury '95, Mining and the Environment* **3,** 989–998.

Wunderly M. D., Blowes D. W., Frind E. O., and Ptacek C. J. (1996) Sulfide mineral oxidation and subsequent reactive transport of oxidation products in mine tailings impoundments: A numerical model. *Wat. Res. Res.* **32(10),** 3173–3187.

Xu C. Y., Schwartz F. W., and Traina S. J. (1997) Treatment of acid-mine water with calcite and quartz. *Env. Eng. Sc.* **14(3),** 141–152.

Xu N., Hochella M. F. Jr., Brown G. E. Jr., and Parks G. A. (1996) Co(II) sorption at the calcite-water interface: I. X-ray photoelectron spectroscopic study. *Geochim. Cosmochim. Acta* **60,** 2801–2815.

Zachara J. M., Kittrick J. A., Dake L. S., and Harsh J. B. (1989) Solubility and surface spectroscopy of zinc precipitates on calcite. *Geochim. Cosmochim. Acta* **53,** 9–19.

Zachara J. M., Cowan C. E., and Resch C. T. (1991) Sorption of divalent metals on calcite. *Geochim. Cosmochim. Acta* **55,** 1549–1562.